Insights into a Single Rod-like Helix in Activated Radixin Required for Membrane−Cytoskeletal Cross-Linking[†]

Klaus P. Hoeflich,[‡] Sachiko Tsukita,[§] Leslie Hicks,[‖] Cyril M. Kay,[‖] Shoichiro Tsukita,[§] and Mitsuhiko Ikura*,[‡]

Division of Molecular and Structural Biology, Ontario Cancer Institute and Department of Medical Biophysics, University of Toronto, 610 University Avenue, Toronto, Ontario M5G 2M9, Canada, Department of Cell Biology, Faculty of Medicine, Kyoto University, Sakyo-ku, Kyoto 606-8501, Japan, and Department of Biochemistry and Protein Engineering Network of Centres of Excellence, University of Alberta, Edmonton, Alberta T6G 2H7, Canada

ABSTRACT: The members of the ezrin−radixin−moesin (ERM) family of proteins function as membrane−cytoskeletal cross-linkers in actin-rich cell surface structures. ERM proteins are thereby thought to be essential for cortical cytoskeleton organization, cell motility, adhesion, and proliferation. These modular polypeptides consist of a central helix-rich region, termed the α-domain, that connects an N-terminal FERM domain required for membrane binding and a C-terminal region which contains a major actin-binding motif. Conformational regulation of ERM protein function occurs by association of the FERM and C-terminal domains, whereby the membrane- and actin-binding activities are mutually suppressed and the protein is thought to take an inactive "closed" form. Here we report *in vitro* and *in vivo* studies of radixin to address the role of the α-domain in conformational activation of ERM proteins. Remarkably, an isolated α-domain comprised of radixin$_{311-469}$ forms a monomeric, stable helical rod that spans 240 Å in length from the N-terminus to the C-terminus, most likely stabilized by extensive salt bridge interactions. By fusing green fluorescent protein variants to the FERM and C-terminal domains, we probed *in vitro* conformational changes impacted by the presence of the α-domain using fluorescence resonance energy transfer (FRET). Furthermore, deletion of this unusually long α-helical structure (radixin residues 314−411) prevents ERM membrane targeting *in vivo*.

Recently, significant progress has been made toward understanding both the structure and function of ERM[1] proteins (*1*, *2*). Ezrin, radixin, and moesin have been shown to join actin filaments to CD43, CD44, and ICAM1-3 cell adhesion molecules and various membrane channels and receptors, such as the Na$^+$/H$^+$ exchanger-3 (NHE3), the cystic fibrosis transmembrane conductance regulator (CFTR), and the β_2-adrenergic receptor. These cross-linking activities are regulated by Rho GTP-binding proteins (*3*). In *Drosophila*, an ERM protein is required for anchoring microfilaments, maintaining cell shape, and coordinating the actin cytoskeleton for proper anteroposterior polarity (*4*). Further analyses of ERM family members have also revealed associations with human disease. For instance, mice lacking radixin are characterized by a breakdown of hepatocyte apical microvilli which ultimately results in mild liver injury similar to human conjugated hyperbilirubinemia in Dubin-Johnson syndrome (*5*). Hamartin, the protein encoded by the tuberous sclerosis complex-1 (TSC1) tumor-suppressor gene, has been linked to ERM proteins in regulating cell adhesion and possibly also hamartoma development (*6*). An ERM-like protein, named merlin, was moreover identified as a tumor suppressor for hereditary neurofibromatosis type-2 (NF2) and holds promise for medical intervention (*1*, *7*). NF2 is an autosomal dominant disease that predisposes individuals to multiple nervous system tumors, including schwannomas, meningiomas, and ependymomas. Mechanistically, loss of merlin expression in NF2-associated schwannoma cells is associated with cell proliferation and dramatic cytoskeletal alterations (*8*).

Once activated downstream of Rho, ERM proteins can be stabilized in an open conformation via phosphorylation of a C-terminal threonine (T564 of radixin; *9*). These phosphorylated ERM proteins can create actin−membrane linkages and are localized to cell-surface structures (*10*). In the cytoplasm, however, a variety of techniques have confirmed that ERM proteins are negatively regulated by association of their FERM and C-terminal domains (CTD) *in vitro* and in living cells (*11−13*). The crystal structure of the FERM−CTD complex has been recently revealed (*14*), although attempts to crystallize full-length ERM proteins or the α-domain alone have been unsuccessful (data not shown). The FERM domain is composed of three subdomains with

* To whom correspondence should be addressed. E-mail: mikura@uhnres.utoronto.ca. Telephone: (416) 946-2025. Fax: (416) 946-2055 or -6529.
‡ University of Toronto.
§ Kyoto University.
‖ University of Alberta.

[1] Abbreviations: CD, circular dichroism; CTD, carboxy-terminal domain; ECFP, enhanced cyan fluorescent protein; EYFP, enhanced yellow fluorescent protein; ERM, ezrin/radixin/moesin; FERM, 4.1/ezrin/radixin/moesin; FRET, fluorescence resonance energy transfer; NF2, neurofibromatosis-2; NMR, nuclear magnetic resonance.
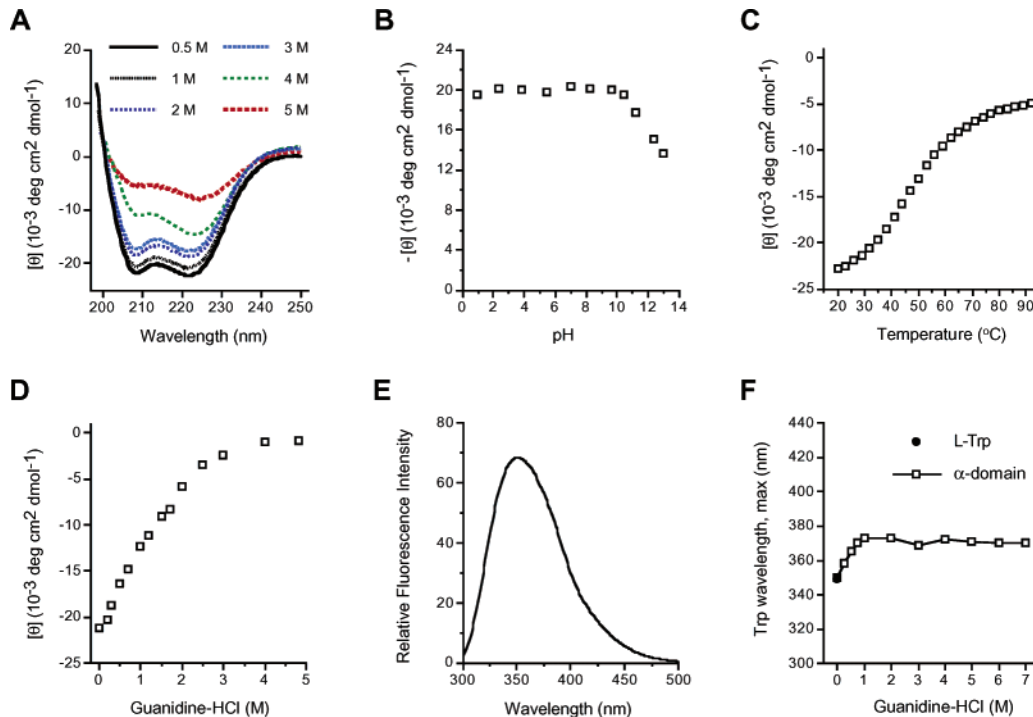
FIGURE 1: Circular dichroism and fluorescence studies of radixin$_{311-469}$. (A and B) Far-UV circular dichroism spectrum of the α-domain at varying NaCl concentrations and pHs as indicated. A representative experiment is shown. (C and D) Temperature and guanidine hydrochloride dependence for α-domain unfolding. Mean molar ellipticity $[\theta]$ is plotted for 222 nm. (E) Radixin tryptophan 445 fluorescence spectrum in aqueous solution. (F) Trp445 (□) and free L-Trp (●) λ_{max} in the presence of increasing guanidine hydrochloride concentrations.

homology in fold to ubiquitin, acyl-CoA binding protein, and the pleckstrin homology domain. The CTD by comparison adopts an extended structure in which the F-actin-binding region is buried in the FERM interface. This well-documented masking model has contributed to this protein family becoming a paradigm for conformational regulation.

Accordingly, questions remain about (i) whether such a long segment of the α-domain (a total of 160 residues) can exist as a single helix in solution and, if so, (ii) how is it possible and (iii) what the role of this central domain is in the conformational activation and other specialized functions of this protein family. There have been several published reports in which models for the α-domain have been described on the basis of secondary structure analysis (*1, 13, 15*). The overwhelming consensus has predicted a heptad hydrophobicity pattern characteristic of coiled-coil proteins with a high propensity for helical dimers. However, this hypothesis has yet to be validated biochemically. Hence, to further enhance our understanding of the structure and function of the α-domain, we have expressed and characterized radixin with α-domain truncations as well as a protein fragment encompassing the radixin α-domain (residues 311–469). In this article, we describe key structural and biological properties of the α-domain and establish the most plausible structural model for this conserved protein domain.

RESULTS

Structural Characteristics of the α-Domain. We first asked whether radixin$_{311-469}$ indeed forms an α-helical structure and, if so, how stable it is. Far-ultraviolet circular dichroism (CD) measurement, to assess the presence of regular secondary structure, indicated that this domain is folded and highly α-helical, with characteristic minima at 222 and 208 nm

(Figure 1A). With increasing temperatures and guanidine-HCl concentrations, the α-domain shows a gradual decrease in α-helical content (as indicated by increasing mean molar ellipticity at 222 nm, $[\theta]_{222}$) and lacks a sharp unfolding transition (Figure 1C,D). This transition is reversible, as shown by the nearly superimposable denaturation and renaturation temperature curves and by the identical spectra at 25 °C before and after denaturation (data not shown), suggesting the α-domain structure is relatively labile and lacks cooperativity in protein folding typical of a globular domain. Furthermore, the midpoint of the temperature dependence (T_m) of the CD signal was measured to be 48 °C and was independent of protein concentration from 10 to 100 μM (data not shown). These results strongly suggest a single helical structure not being dictated by self-association.

Our preliminary NMR studies on ^{15}N-labeled radixin$_{311-469}$ using ^{15}N$-^{1}$H heteronuclear single-quantum coherence spectroscopy (HSQC) yielded spectra with a broad appearance under various conditions (data not shown). As a result of this protein aggregation, radixin$_{311-469}$ is not amenable to high protein concentrations (~1 mM) that are suitable for NMR spectroscopy. In an attempt to optimize buffer conditions, temperature (15–30 °C), pH (3.0–4.2 and 6.5–7.6), salts with varying Hofmeister effects, and additives with published beneficial effects on α-helical protein stability (CHAPS zwitterionic detergent and amino acids with charged side chains) were tested. However, none of these conditions dramatically improved the HSQC spectrum. Preliminary protein crystallization screens also did not yield positive results (data not shown).

Thus, to estimate the shape of the radixin$_{311-469}$ α-domain, we employed analytical ultracentrifugation to obtain first-principle hydrodynamic information (Figure 2A). Sedimenta-
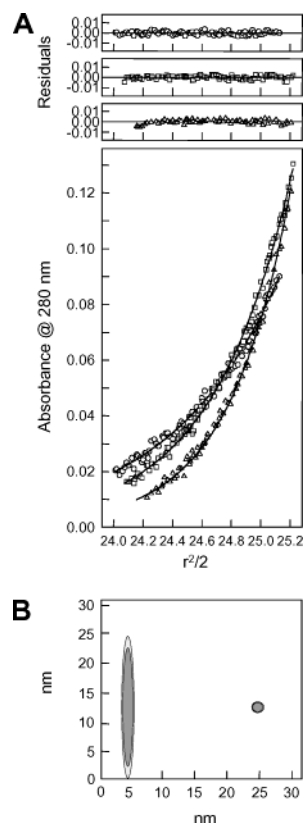
FIGURE 2: Hydrodynamic characterization and prolate ellipsoid modeling of radixin$_{311-469}$. (A) Sedimentation equilibrium data for the α-domain fit globally to a single-species model. α-Domain (0.18 mg/mL) was analyzed at 25 °C and three speeds: 24 000 (○), 28 000 (□), and 32 000 rpm (△). Lower panels display (radial distance)^2/2 vs absorbance plots. Symbols represent measured data points, and solid lines represent theoretical fit lines. Upper panels display the random deviation of the data points from the fit lines, indicating a good fit to the model. The calculated apparent molecular weight of 20 336 agreed well with the theoretical monomer α-domain molecular weight. Additional loading concentrations of 0.59 and 0.35 mg/mL revealed identical results (data not shown). (B) Hydrated prolate ellipsoid model of the α-domain produced using SEDNTERP illustrating the calculated shape and size of the protein, including the contribution from hydration (outer boundary). The side view (left) and view looking down the central axis (right) are shown.

tion equilibrium data were evaluated using the NONLIN program, which incorporates a nonlinear least-squares curve fitting algorithm (*16*). The experimentally ascertained sedimentation coefficient ($s°_{20,w}$), the partial specific volume, the molecular weight, and a predetermined hydration factor (*17*) were used with SEDNTERP software to calculate the dimensions of the molecule based on a prolate ellipsoid model (*18, 19*). Figure 2B presents a graphical representation of this model with hydration shown as a separate layer. Accordingly, the α-domain is asymmetric (24.2 nm × 1.9 nm). The axial ratio (major axis/minor axis) was determined to be 12.9, whereas in comparison, a globular protein such as BSA has an axial ratio of 2.6 (*20*). Proteins that are asymmetric in nature will sediment more slowly than compact globular proteins because of an increased frictional coefficient. Our sedimentation velocity results were consistent with this hydrodynamic model as radixin$_{311-469}$ had a low intrinsic sedimentation coefficient of 1.334 S. We conclude that the α-domain is an obligate monomer and forms a long, helical rod.

Rationale for the Long Rod Structure. Although α-helices can vary considerably in length, the 240 Å α-domain far exceeds the average length of helices (~15 Å) found in globular proteins. This raises the interesting question as to how this extended structure is stabilized. Our careful inspection of the α-domain sequences among ERM family members revealed the presence of a large number of conserved acidic and basic amino acid pairs (a total of 53) available for electrostatic interactions and surface salt bridges between residue i and residue $i + 3$ or 4 (Figure 3A). While typically there are only a few salt bridges in proteins and the free energy contribution of an individual surface-exposed salt bridge is small (0.5 kcal/mol), the network and complexity of the α-domain bridges are predicted to contribute synergistically to its thermal stability (*21, 22*). This can be further appreciated by a comparative analysis in which potential salt bridges are compared with other proteins such as two- and three-helix bundles (Max and α-spectrin, respectively) and the globular helical protein, hemoglobin (Figure 3B). If these bridges are crucial for maintaining the secondary structure of the α-domain, a high ionic strength should diminish the stability of the helix. Indeed, the α-helical fold is highly dependent on salt concentration (Figure 1A). These results are reminiscent of those from peptides containing tandem salt bridges that are quite sensitive to charge screening due to many interacting charged groups in proximity (*21, 23*). The radixin$_{311-469}$ α-domain structure is furthermore responsive to pH titration, as the state of ionization of side chains clearly controls the ability to form ion pairs (Figure 1B). Finally, tryptophan fluorescence was used to probe for denaturation-induced tertiary structure alterations showing the single Trp445 is fully solvent exposed, consistent with this domain being a single helix (Figure 1E,F).

Given the structural model of a single helix which is placed spanning the FERM and C-terminal domain structures as determined by X-ray crystallography (*14, 24*; Figure 3C), how is it that the α-domain can enable intramolecular interaction of the FERM and C-terminal domains? Partial trypsinization of purified radixin$_{311-469}$ revealed two stable intermediate products that were identified using mass spectrometry and N-terminal sequencing (Figure 3D). Preferential proteolytic cleavage was shown to occur at exposed sites in the N-terminal portion of the α-domain (after residues 331 and 352 of radixin). Hence, unwinding of the helix through these residues would confer sufficient polypeptide flexibility and length for the radixin termini to "fold" back to one another, thereby reconciling this model with the inactive monomer conformation.

Interestingly, while the domain architecture of the tumor suppressor NF2/merlin is similar to that of radixin and has been suggested to function via an analogous molecular mechanism, its α-domain contains significantly fewer charged amino acids, and therefore, the propensity for salt bridging would appear to be weaker. This could suggest different structural and dynamic properties of this central linker domain and may partially explain some of the unique cellular and biochemical features of NF2/merlin (*1*).

Role of the α-Domain in ERM Conformation and Subcellular Localization. To assess the previously described "open−closed" model for ERM protein activation (*1, 2*), further biochemical and cell-based approaches were applied.
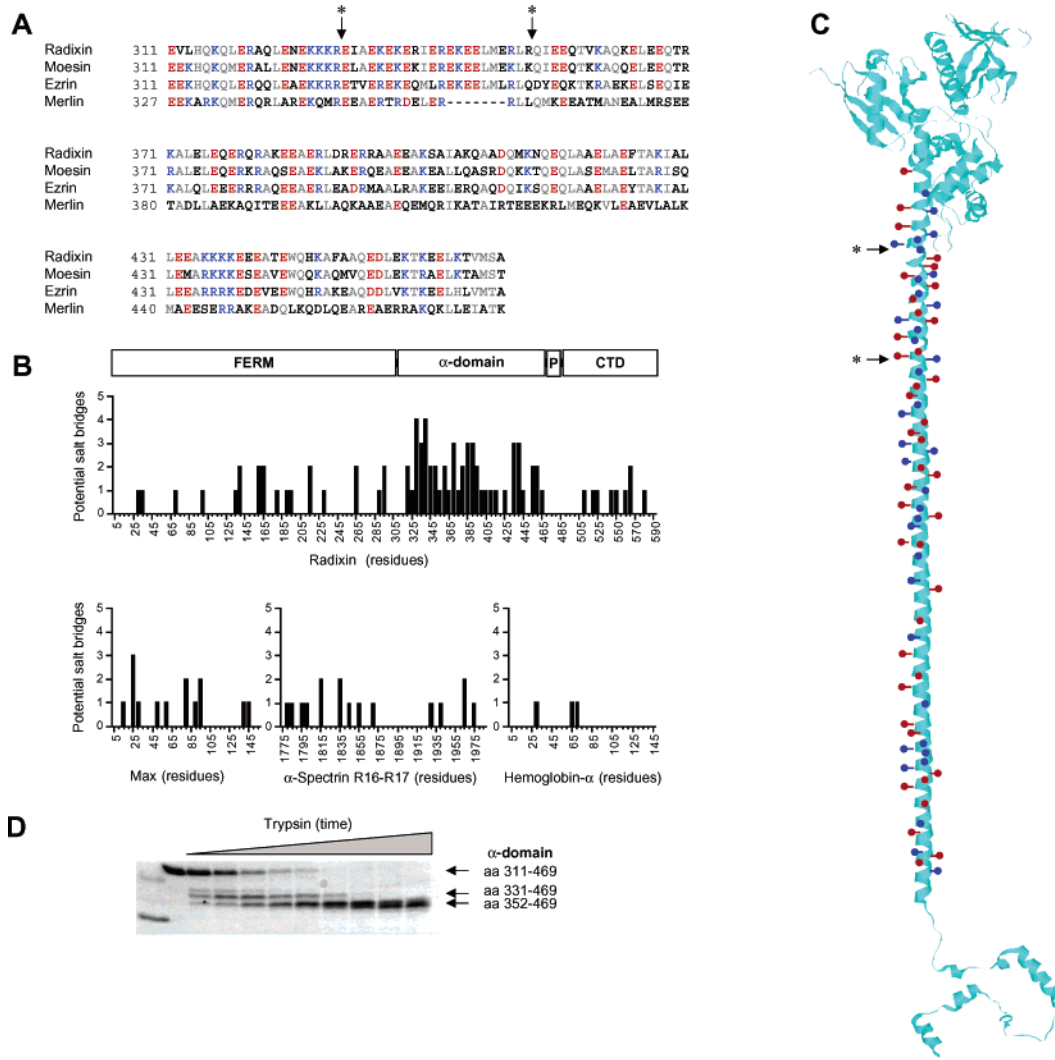
FIGURE 3: Residues of the radixin α-domain available for electrostatic interactions and surface salt bridges. (A) Sequence alignment of murine ERM protein α-domains. Positively (blue) and negatively (red) charged residues are highlighted. Protease-sensitive sites are denoted with asterisks. (B) Proposed helix-stabilizing, intramolecular salt bridge interactions for radixin, a helical dimer (Max), trimer (α-spectrin repeats 16 and 17), and a globular helical protein (hemoglobin-α). The number of predicted electrostatic interactions occurring between residues i and $i + 3$ or between residues i and $i + 4$ is shown for the y-axis. NCBI accession numbers are CAA43087, AAA36200, AAA51790, and 620479A, respectively. (C) Model of radixin structure based on experimentally derived α-domain features. FERM and CTD are Protein Data Bank (PDB) entries 1E5W and 1EF1, respectively. Positively and negatively charged residues are shown in blue and red, respectively. (D) Partial proteolysis of radixin$_{311-469}$ identifies a flexible region. Polypeptides were characterized using mass spectrometry and N-terminal sequencing.

With the aim of monitoring conformational changes by fluorescence resonance energy transfer (FRET), we generated bacterial expression vectors for cyan fluorescent protein (ECFP) and yellow fluorescent protein (EYFP) fusions of the FERM, C-terminal domain, and full-length radixin (Figure 4A). FRET here occurs by energy transfer from an excited ECFP donor to an EYFP acceptor through a nonradiative dipole−dipole interaction (25, 26). First, we tested the feasibility of this approach in ascertaining FERM and C-terminal domain association, as existing in the inactive ERM conformation (Figure 4B). In comparison to ECFP− FERM emission alone, the addition of equimolar CTD− EYFP yielded an increase in acceptor emission, centered at 526 nm, accompanied by a decrease in donor emission intensity at 476 nm. This change is ascribed to energy transfer as acceptor and donor emission have an inverse relationship due to ECFP quenching upon FRET with EYFP. To then further verify that changes in FRET efficiency are dependent on interdomain binding, a phosphorylation-mimicking mutant

of a key regulatory phosphorylation site, Thr564, was used. Phosphorylation of this C-terminal threonine contributes to weakening of the FERM−CTD interaction presumably by both electrostatic and steric effects (14). As expected, the emission spectrum of the ECFP−FERM−CTD^{T564E}−EYFP complex showed a corresponding reduction of the magnitude of the YFP specific emission peak. Importantly, these FRET binding assays are in good agreement with parallel pulldown experiments carried out with the same proteins (Figure 4C). Given these characteristics, the chimeras represent favorable donor−acceptor pairs for monitoring spatial proximity and distance relationships between the FERM and C-terminal domains of radixin by FRET.

There is a strong inverse relationship between FRET and chromophore separation so that efficient FRET occurs only if the donor and acceptor are within $10-100$ Å of each other. Hence, FRET can be further used to measure radixin FERM−CTD interdomain distances in the presence or absence of the α-domain (Figure 4D). Here FRET is reported
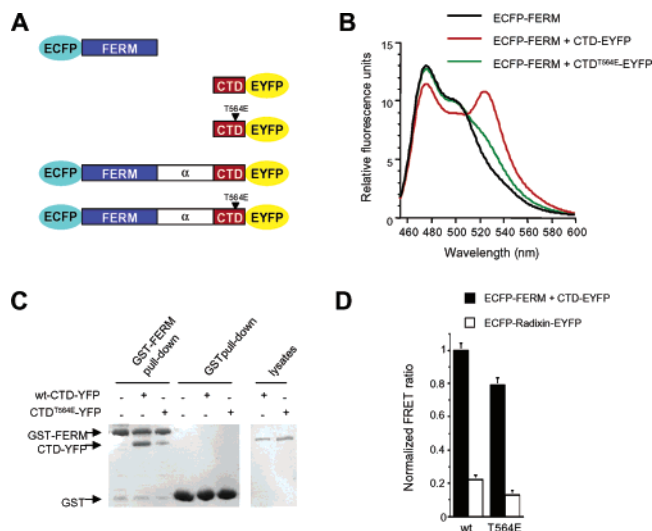
FIGURE 4: α-Domain diminishes the level of association of FERM and C-terminal domains *in vitro*. (A) Schematic representation of radixin FRET constructs. (B) Fluorescence spectra of purified fusion proteins. The total protein concentration for each sample was adjusted to 2.5 μM. Samples of ECFP−FERM alone (black) and with CTD−EYFP (red) or CTD[T564E]−EYFP (green) were excited at 437 nm and emission spectra recorded. (C) Association of GST−FERM or GST alone monitored by electrophoresis in 15% polyacrylamide gels. For characterization of FERM/CTD affinities, ECFP (27 kDa) was substituted with glutathione *S*-transferase (GST, 28 kDa), and complexes were purified on glutathione−Sepharose. (D) FRET emission ratio for isolated domains and full-length radixin. Results are normalized against ECFP−FERM with CTD−EYFP and shown as the mean $\pm$ the standard deviation of three independent experiments.

as a ratio of EYFP to ECFP emission during ECFP excitation, where higher emission ratios indicate an increased efficiency of FRET. A significant decrease (∼5-fold) in the level of FRET relative to the mixture of isolated domains was measured for full-length radixin, where the central α-domain separates the terminal domains. The T564E substitution causes a further 20% reduction in the level of FRET in either full-length or individual domain scenarios. This diminishing of the level of FRET by the α-domain implies a great increase in chromophore distance, and accordingly also of FERM and C-terminal domains, as dictated by Förster's equation (*27*). Accordingly, partial relaxing of the α-domain at greater ionic strengths (Figure 1A) resulted in an increase in the level of FRET (data not shown). These distance estimates assume that the relative orientation and mobility of ECFP and EYFP are unchanged in the full-length radixin chimera. The residual FRET observed for the ECFP−radixin−EYFP species can be explained by intermolecular FERM−CTD complexes present in low abundance at 2.5 μM protein or the well-established propensity of GFP family members to oligomerize (*26*). Hence, with regard to the overall dimensions of the α-domain described herein, the change in apparent distance between the fluorophores can be interpreted as a conversion from a closed to a significantly more open conformation in molecules containing the long α-domain.

As radixin mutations mimicking Thr564 phosphorylation have been shown to result in the formation of persistent actin-based microvillar structures (*1, 2*), full-length, 50% α-domain-deleted, and 92% α-domain-deleted (residues 314−411 and 314−461, respectively) chromophore-tagged radixin[T564E]

constructs were expressed in murine fibroblastic L cells, and the cellular morphology and cytoskeletal organization were visualized by DeltaVision deconvolution fluorescence microscopy. Full-length and Δ314−411 radixin[T564E] are concentrated with endogenous ERM proteins in cortical microvillar structures (Figure 5A). However, upon further truncation of the α-domain, radixin remains diffusely distributed in the cytoplasm and recruitment of the cytoskeleton is not observable. Correspondingly, transfected full-length and Δ314−411, but not Δ314−461, radixin[T564E] chimeras precisely colocalized with cell surface actin (Figure 5B). These data suggest that the α-domain is needed for conformational activation of ERM proteins *in vivo* and are consistent with ERM regulation involving separation of the FERM and C-terminal domains, a plausible function for the α-domain. By sustaining the unmasked, open conformation, the α-domain may also play a role in enabling ERM-binding proteins to make contact with the terminal globular domains.

DISCUSSION

Previous studies on ERM proteins have focused on the globular FERM and C-terminal regions with little attention on the α-domain. We found that *in vivo*, the α-domain is required for regulating the formation of the functional cortical layer, including actin binding to the membrane and possibly the organization of membrane transporters or channels. Our analysis has established a set of structural constraints for which the only feasible model points to the α-domain being an extremely long, linear monomer with an enhanced number of electrostatic, salt bridge interactions predicted to contribute synergistically to its thermal stability.

How can these observations be integrated into the action of the whole protein? Our exploration of the α-domain structure leads to a dynamic mechanism of ERM activation, represented by a tunable switch as opposed to an on−off switch (Figure 6). The tunable switch model involves relatively subtle thermodynamic changes between the conformational states, and both closed and open conformations can coexist in a population. While physical interaction of the isolated FERM domain and CTD produces a highly stable complex, as evidenced by the X-ray structure (*14*), insertion of the long, rod-like α-domain increases the free energy of the full-length protein and largely destabilizes the closed conformation. Moreover, our fluorescence resonance energy transfer (FRET) experiments show that while the isolated FERM domain and CTD produce a strong FRET enhancement, the value for the full-length protein corresponding to the closed conformation is significantly smaller (Figure 4D). Also, the T564 mutant, corresponding to the open form, does not abolish FRET completely under the conditions that were tested, indicating that the T564E mutant can assume the closed or open conformation and the observable represents a time average between the two forms. These data suggest less binary (on−off) behavior in exchange between closed and open conformations. In a given cell, the relative populations of the two conformations must be balanced by various factors such as phosphorylation and phosphoinositide binding, which induce subtle changes in the free energy of the ERM conformations. For the closed conformation, the data are congruent with both monomer and dimer models. The flexibility of the α-domain necessitated by the monomer conformation is supported by radixin[311−469] proteolysis data
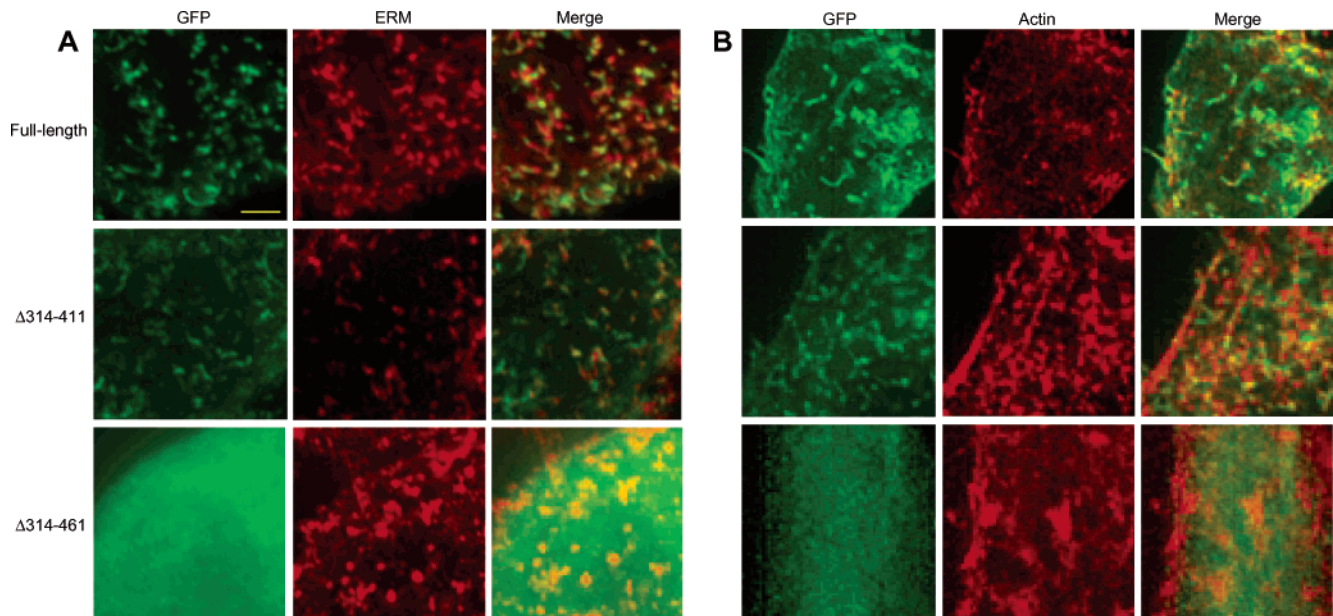
FIGURE 5: Immunofluorescence micrographs indicating the α-domain is required for membrane localization and actin binding. (A) L cells were transfected with the indicated constructs and double stained with anti-ERM and anti-GFP antibodies. Full-length and Δ314−411 radixin[T564E] (green) are recruited together with endogenous ERM proteins (red) to cell surface structures, while in contrast, radixin[T564E]Δ314−461 is diffusely distributed in the cytoplasm. (B) Full-length and Δ314−411, but not Δ314−461, radixin[T564E] (green) were precisely colocalized with actin in microvilli as determined by staining for phalloidin (red), an actin cytoskeleton marker. The scale bar is 2.5 μm long.
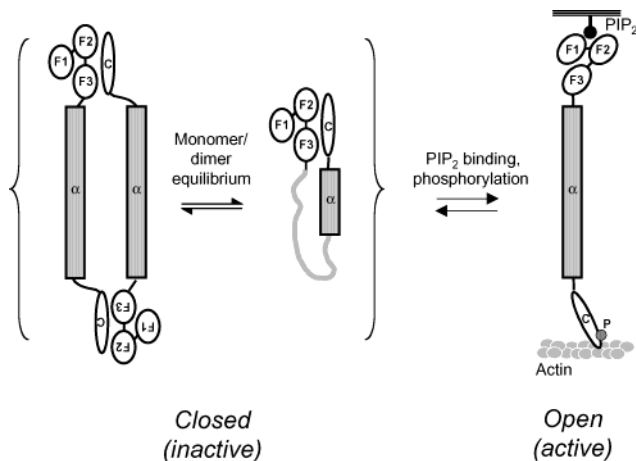

FIGURE 6: Revised model for ERM protein activation. See the text for details. F1 is the four-point one/ezrin/radixin/moesin (FERM) subdomain, α the α-domain, C the carboxy-terminal domain, P phosphorylation, and PIP_2 phosphatidylinositol 3,4-bisphosphate.

(Figure 3D) pointing to melting of the 47 N-terminal residues. The resulting unfolded coil would be sufficiently long to allow for intramolecular association of FERM with CTD. In the dimer case, intermolecular FERM−CTD interaction is the cause of dimerization and no direct interaction between α-domains is involved. In either case, we propose that the α-domain plays a key role in our proposed ERM activation mechanism involving a tunable conformational switch. In essence, the α-domain primarily acts as a "suppressor" domain for the inactive conformation, and upon stimulation, it can modulate the functions of membrane-anchoring (FERM) and actin-binding (CTD) domains.

It is surprising that a single helix of such length exists in a monomeric protein. One may speculate that its length is important for shaping cell surface structures or that the dipole moment of the helix may even facilitate interaction of the radixin N-terminus with the negatively charged phospholipid bilayer. Further examination of its biological functions is currently underway with an aim to developing *in vivo* FRET tools for this interesting protein family.

MATERIALS AND METHODS

Protein Expression and Purification. The α-domain (residues 310−469) of murine radixin was cloned into a histidine-tagged pET15b vector (Novagen) using oligos 5′-CAT ATG GAG GTT TTG CAT CAG AAG CA-3′ and 5′-GGA TCC TCA CGC AGA CAT CAC AGT TTT TA-3′. Following overnight induction with 0.4 mM IPTG at 17 °C in BL21-(DE3)pLysS *Escherichia coli* cells, the cells were disrupted by sonication at 277 K, and the supernatant was applied onto nickel affinity resin (Qiagen). The protein was washed, eluted, and then cleaved with human thrombin at 10 units/mL in 20 mM Tris (pH 7.6), 100 mM NaCl, 2.5 mM $CaCl_2$, and 1 mM DTT for 14 h at room temperature. The cleaved protein was collected for further purification with a Hitrap Q column chromatographic step (Pharmacia Biotech). Purity was monitored by 15% polyacrylamide gel electrophoresis. For FRET analyses, CFP and YFP chimeras of radixin proteins were cloned into *Bam*HI−*Eco*RI-cleaved pRSETc (Invitrogen) for purification via a His_6 tag.

Analytical Ultracentrifugation. Sedimentation equilibrium experiments were carried out in a Beckman XL-I analytical ultracentrifuge. Aliquots were loaded into six-sector CFE sample cells, allowing three concentrations of a sample to be run simultaneously. Runs were performed at a minimum of two different speeds, and each speed was maintained until there was no significant difference in $r^2/2$ versus absorbance scans taken 2 h apart to ensure that equilibrium was achieved. The sedimentation velocity data were analyzed to determine sedimentation coefficients using the program SVEDBERG (*19*), which incorporates a modified Fujita−MacCosham function into a nonlinear least squares fitting routine to adjust

the sedimentation boundaries to either single-species or multiple-species models. The program SEDNTERP was employed to calculate the protein's partial specific volume, $S_{20,w}$, axial ratio, and the solvent density and viscosity using calculations described in detail by Laue et al. (*18*).

Circular Dichroism and Fluorescence Studies. Far-UV spectra were recorded using an Aviv circular dichroism spectrometer (model 62 DS). Samples were prepared in 20 mM NaH_2PO_4 under the indicated NaCl and pH conditions in 0.1 cm quartz cuvettes. Thermal and chemical denaturation curves were prepared by monitoring ellipticity at 222 nm as a function of temperature or guanidine concentration. *In vitro* fluorescence spectra were collected using a Shimadzu RF-5301 spectrofluorophotometer with a slit width giving a resolution of 1 nm. FRET values were normalized for basal YFP excitation at 476 nm.

NMR Spectroscopy Measurements. All $^1H-^{15}N$ hetero-nuclear single-quantum coherence (HSQC) NMR experiments were performed between 15 and 30 °C on a Varian Unity Inova 500 MHz spectrometer. Purified radixin$_{311-469}$ samples were concentrated to 0.5 mL with a final protein concentration of approximately $0.4-1.0$ mM. All NMR data were processed using NMRPipe and NMRDraw.

Transfection and Microscopy. Deletion constructs of the α-domain were constructed by ligation of *Sac*II sites using oligos 5′-TCC CCG CGG ATG CAA AAC CTC CCG GGC CTG AGC CT-3′ and 5′-TCC CCG CGG ATG AAG AAC CAG GAG CAG CTG GCA GCA-3′ or 5′-TCC CCG CGG GAA GAG CTA AAA ACT GTG ATG TCT GCG CCA CCT-3′ for Δ314−411 and Δ314−461, respectively. Fibroblastic L cells were transfected with ECFP- and EYFP-tagged pCDNA3 (Invitrogen) constructs encoding radixin^{T564E}, radixin^{T564E}Δ314−411, or radixin^{T564E}Δ314−461 using Lipofectamine (GIBCO BRL) and cultured overnight. Cells were fixed with 2% formalin in PBS and treated with 0.2% Triton X-100 for 15 min. Cellular proteins were visualized with Alexa564-phalloidin (Molecular Probes, Inc.), anti-GFP polyclonal antibody (Medical Biological Laboratories), or rat monoclonal ezrin and moesin antibodies (*28*). Specimens were observed using an Olympus IX70 microscope with appropriate combinations of filters and mirrors, and images were processed by DeltaVision restoration (Applied Precision).

ACKNOWLEDGMENT

REFERENCES

1. Bretscher, A., Edwards, K., and Fehon, R. G. (2002) ERM proteins and merlin: integrators at the cell cortex, *Nat. Rev. Mol. Cell Biol. 3*, 586−599.
2. Tsukita, S., and Yonemura, S. (1999) Cortical actin organization: lessons from ERM (ezrin/radixin/moesin) proteins, *J. Biol. Chem. 274*, 34507−34510.
3. Hirao, M., Sato, N., Kondo, T., Yonemura, S., Monden, M., Sasaki, T., Takai, Y., Tsukita, S., and Tsukita, S. (1996) Regulation mechanism of ERM (ezrin/radixin/moesin) protein/plasma membrane association: possible involvement of phosphatidylinositol turnover and Rho-dependent signaling pathway, *J. Cell Biol. 135*, 37−51.
4. Polesello, C., Delon, I., Valenti, P., Ferrer, P., and Payre, F. (2002) Dmoesin controls actin-based cell shape and polarity during *Drosophila melanogaster* oogenesis, *Nat. Cell Biol. 4*, 782−789.
5. Kikuchi, S., Hata, M., Fukumoto, K., Yamane, Y., Matsui, T., Tamura, A., Yonemura, S., Yamagishi, H., Keppler, P., Tsukita, S., and Tsukita, S. (2002) Radixin deficiency causes conjugated hyperbilirubinemia with loss of Mrp2 from bile canalicular membranes, *Nat. Genet. 31*, 320−325.
6. Lamb, R. F., Roy, C., Diefenbach, T. J., Vinters, H. V., Johnson, M. W., Jay, D. G., and Hall, A. (2000) The TSC1 tumour suppressor hamartin regulates cell adhesion through ERM proteins and the GTPase Rho, *Nat. Cell Biol. 2*, 281−287.
7. Reed, N., and Gutmann, D. H. (2001) Tumorigenesis in neurofibromatosis: new insights and potential therapies, *Trends Mol. Med. 7*, 157−162.
8. Bashour, A. M., Meng, J. J., Ip, W., MacCollin, M., and Ratner, N. (2002) The neurofibromatosis type 2 gene product, merlin, reverses the F-actin cytoskeletal defects in primary human Schwannoma cells, *Mol. Cell. Biol. 22*, 1150−1157.
9. Bretscher, A. (1989) Rapid phosphorylation and reorganization of ezrin and spectrin accompany morphological changes induced in A-431 cells by epidermal growth factor, *J. Cell Biol. 108*, 921−930.
10. Hayashi, K., Yonemura, S., Matsui, T., and Tsukita, S. (1999) Immunofluorescence detection of ezrin/radixin/moesin (ERM) proteins with their carboxyl-terminal threonine phosphorylated in cultured cells and tissues, *J. Cell Sci. 112*, 1149−1158.
11. Gary, R., and Bretscher, A. (1995) Ezrin self-association involves binding of an N-terminal domain to a normally masked C-terminal domain that includes the F-actin binding site, *Mol. Biol. Cell 6*, 1061−1075.
12. Magendantz, M., Henry, M. D., Lander, A., and Solomon, F. (1995) Interdomain interactions of radixin in vitro, *J. Biol. Chem. 270*, 25324−25327.
13. Andreoli, C., Martin, M., Le Borgne, R., Reggio, H., and Mangeat, P. (1994) Ezrin has properties to self-associate at the plasma membrane, *J. Cell Sci. 107*, 2509−2521.
14. Pearson, M. A., Reczek, D., Bretscher, A., and Karplus, P. A. (2000) Structure of the ERM protein moesin reveals the FERM domain fold masked by an extended actin binding tail domain, *Cell 101*, 259−270.
15. Sun, C. X., Robb, V. A., and Gutmann, D. H. (2002) Protein 4.1 tumor suppressors: getting a FERM grip on growth regulation, *J. Cell Sci. 115*, 3991−4000.
16. Johnson, M. L., Correia, J. J., Yphantis, D. A., and Halvorson, H. R. (1981) Analysis of data from the analytical ultracentrifuge by non-linear least-squares techniques, *Biophys. J. 36*, 575−588.
17. Kumosinski, T. F., and Pessen, H. (1982) Estimation of sedimentation coefficients of globular proteins: an application of small-angle X-ray scattering, *Arch. Biochem. Biophys. 219*, 89−100.
18. Laue, T. F., Shah, B. D., Ridgeway, T. M., and Pelletier, S. L. (1991) in *Analytical Ultracentrifugation in Biochemistry and Polymer Science* (Harding, S. E., Rowe, A. J., and Horton, J. C., Eds.) pp 90−125, Royal Society of Chemistry, Cambridge, U.K.
19. Philo, J. S. (1999) *Svedberg*, version 6.23, 3329 Heatherglow Ct., Thousand Oaks, CA.
20. Mani, R. S., Karimi-Busheri, F., Cass, C. E., and Weinfeld, M. (2001) Physical properties of human polynucleotide kinase: hydrodynamic and spectroscopic studies, *Biochemistry 40*, 12967−12973.
21. Smith, J. S., and Scholtz, J. M. (1998) Energetics of polar side-chain interactions in helical peptides: salt effects on ion pairs and hydrogen bonds, *Biochemistry 37*, 33−40.
22. Lyu, P. C., Gans, P. J., and Kallenbach, N. R. (1992) Energetic contribution of solvent-exposed ion pairs to alpha-helix structure, *J. Mol. Biol. 223*, 343−350.
23. Olson, C. A., Spek, E. J., Shi, Z., Vologodskii, A., and Kallenbach, N. R. (2001) Cooperative helix stabilization by complex Arg-Glu salt bridges, *Proteins 44*, 123−132.
24. Edwards, S. D., and Keep, N. H. (2001) The 2.7 Å crystal structure of the activated FERM domain of moesin: an analysis of structural changes on activation, *Biochemistry 40*, 7061−7068.
25. Truong, K., and Ikura, M. (2001) The use of FRET imaging microscopy to detect protein−protein interactions and protein conformational changes in vivo, *Curr. Opin. Struct. Biol. 11*, 573−578.
26. Zhang, J., Campbell, R. E., Ting, A. Y., and Tsien, R. Y. (2002) Creating new fluorescent probes for cell biology, *Nat. Rev. Mol. Cell Biol. 3*, 906−918.

27. Förster, T. (1951) *Fluoreszenz Organischer Verbindungen*, Vandenhoeck and Ruprecht, Göttingen, Germany.

28. Yonemura, S., Matsui, T., Tsukita, S., and Tsukita, S. (2002) Rho-dependent and -independent activation mechanisms of ezrin/radixin/moesin proteins: an essential role for polyphosphoinositides in vivo, *J. Cell Sci. 115*, 2569−2580.